Article

Tunable High-Static-Low-Dynamic Stiffness Isolator under Harmonic and Seismic Loads

Giovanni Iarriccio [1,*], Antonio Zippo [1], Fatemeh Eskandary-Malayery [2], Sinniah Ilanko [2], Yusuke Mochida [2], Brian Mace [3] and Francesco Pellicano [1]

[1] Department of Engineering "Enzo Ferrari", University of Modena and Reggio Emilia, Via Vivarelli 10, 41125 Modena, Italy; antonio.zippo@unimore.it (A.Z.); francesco.pellicano@unimore.it (F.P.)

[2] School of Engineering, University of Waikato, Hamilton 3216, New Zealand; fe14@students.waikato.ac.nz (F.E.-M.); ilanko@waikato.ac.nz (S.I.); yusuke@waikato.ac.nz (Y.M.)

[3] Department of Mechanical and Mechatronics Engineering, University of Auckland, Auckland 1030, New Zealand; b.mace@auckland.ac.nz

* Correspondence: giovanni.iarriccio@unimore.it

Abstract: High-Static-Low-Dynamic Stiffness (HSLDS) mechanisms exploit nonlinear kinematics to improve the effectiveness of isolators, preserving controlled static deflections while maintaining low natural frequencies. Although extensively studied under harmonic base excitation, there are still few applications considering real seismic signals and little experimental evidence of real-world performance. This study experimentally demonstrates the beneficial effects of HSLDS isolators over linear ones in reducing the vibrations transmitted to the suspended mass under near-fault earthquakes. A tripod mechanism isolator is presented, and a lumped parameter model is formulated considering a piecewise nonlinear–linear stiffness, with dissipation taken into account through viscous and dry friction forces. Experimental shake table tests are conducted considering harmonic base motion to evaluate the isolator transmissibility in the vertical direction. Excellent agreement is observed when comparing the model to the experimental measurements. Finally, the behavior of the isolator is investigated under earthquake inputs, and results are presented using vertical acceleration time histories and spectra, demonstrating the vibration reduction provided by the nonlinear isolator.

Keywords: high-static-low-dynamic stiffness; vibration isolators; experiments; transmissibility; earthquakes

1. Introduction

Each year, over a million seismic events and the resulting large number of fatalities pose a challenge to the human population [1]. The development of new building technologies and early warning and prevention systems can counter the disastrous effects of earthquakes. In this framework, exploiting the inherent nonlinearities of seismic isolation systems represents a possible approach to developing high-performance devices for preventing buildings from undergoing disastrous damage during seismic events.

Vibration isolation systems can be classified as active or passive based on the presence or absence of integrated actuators for real-time operation. However, during seismic events, sudden power supply outages may occur, making active vibration control systems unreliable. Passive vibration isolators, functioning without external power or control, provide a cost-effective, robust, and reliable means of isolating buildings from ground motion [2].

Concerning the transmissibility of a linear suspension under harmonic base excitation, a standard mass-spring system allows for vibration isolation (i.e., absolute transmissibility amplitude $T < 1$) when the forcing frequency exceeds $\sqrt{2km^{-1}}$, where k and m denote the stiffness and mass of the system, respectively [3]. Thus, a low stiffness is desired to increase the working frequency range, but it results in larger static deflection, which may be impractical in some applications. To circumvent this issue, quasi-zero stiffness

(QZS) mechanisms, also known as zero spring rate mechanisms (ZSRMs) or High-Static-Low-Dynamic Stiffness mechanisms (HSLDS), can extend the working frequency range by leveraging kinematic nonlinearities. While effective, their performance is sensitive to mistuning [4], wherein any deviation in geometry or static loading from the structure (or payload) can alter the dynamic characteristics of the system, and it is worthwhile to note that the use of nonlinear isolators, which rely on the negative stiffness concept, is limited to applications where the mass of the payload is small, as these systems require a force preload of the same order of the payload weight [5].

In the analysis presented herein, only the mitigation of ground vibrations in the vertical directions is addressed. Studies in which HSLDS systems have been used to mitigate horizontal vibrations can be found in [6,7].

The HSLDS isolator considered here is based on an oscillating mass supported by a vertical linear spring in parallel with one or more horizontal linear springs. In dynamic conditions, the horizontal springs contribute to the equivalent dynamic vertical stiffness for small amplitude motions by reducing the stiffness and introducing hardening nonlinearities. The former effect increases the isolator working range, while the latter leads to jump-up/jump-down phenomena close to the saddle-node bifurcation points and reduces the isolation region since the resonance peak moves toward higher frequencies [8].

One of the early works on the subject was presented by Molyneux [9], where the arrangement of inclined springs was proposed to reduce the equivalent stiffness of a system. Many potential applications were suggested for road vehicle suspensions, torsional couplings, and vibration sensors. Woodard et al. [10] focused on the transition from linear to nonlinear behavior of a ZSRM mechanism. Considering the system around the equilibrium position, the authors demonstrated that increasing the cable preload decreases overall vertical stiffness, reducing the system's natural frequencies. Platus et al. [7] presented a series of isolators with multiple degrees of freedom capable of suppressing both vertical and horizontal oscillations. Comprehensive theoretical studies on the static analysis and nonlinear dynamics of QZS mechanisms are provided in Refs. [11–15], where force-displacement expressions and nonlinear equations of motion are derived, solved, and discussed for various configurations, parameters, and different forcing functions.

It is well established that an HSLDS system can be frequently modeled by the Duffing equation, where damping terms are added to simulate different dissipation mechanisms. Cheng et al. [16,17] and Shahraeeni et al. [18] considered a QZS system with linear viscous dampers. The resulting nonlinear damping has been approximated by terms like $\dot{x}x^n$, i.e., velocity times the n-th power of the displacement, in agreement with the lumped-mass system consisting of two angled dashpots considered in Ref. [19]. Den Hartog [20] and Ravindra and Mallik [21] addressed the role of dry friction on the dynamics of oscillators under base excitation, considering linear or nonlinear cubic stiffness terms. Donmez et al. [22] proposed the introduction of a dry friction element inside the isolator to reduce the transmissibility for frequencies around the resonance region. Liu and Yu [23] presented a QZS system with an oscillating mass supported by a vertical spring and surrounded by four lateral springs. Despite poor agreement between analytical and experimental results, attributed to a stiffness increment induced by the bending stiffness of the lateral springs not being considered in the theoretical model, experiments have shown a transmissibility reduction compared with the linear oscillator, confirming the effectiveness of the QZS system and the need to go beyond the classical model to predict QZS isolator performance.

The number of studies on QZS/HSLDS systems is increasing, reflecting growing interest in the topic [24]. Further theoretical and experimental studies can be found in the literature, proposing active stiffness control strategies [25], nonlinear absorbers [26], non-conventional springs [27], piecewise restoring forces [28], magnets [29,30], bio-inspired isolators [31], and X-shaped mechanisms [32,33] to avoid instabilities and expand the QZS working range.

In a recent study [34], theoretical and experimental results for a small-scale two-dimensional HSLDS isolator subjected to amplitude-scaled actual vertical earthquake

signals were presented, demonstrating the isolator's effectiveness in reducing acceleration transmission under near-fault earthquakes. Based on these results, the present study investigated the behavior of a tunable HSLDS isolator for sensitive equipment under vertical base excitation. The design of a three-dimensional mechanism is proposed, and the fundamental components of the prototype under analysis are described. A theoretical model is formulated, incorporating piecewise restoring forces and Coulomb dry friction. The experimental analysis aims to evaluate the ground motion reduction achievable using such a device. To conduct the experiments, a high-power electrodynamic shaking table was utilized. The isolator's transmissibility was evaluated through harmonic base excitation tests, and a direct comparison with a linear suspension was made under replicated near-fault earthquakes, demonstrating the beneficial effects of the HSLDS isolator.

2. Description of the Real Isolator and Theoretical Dynamic Model

Figure 1a,b show the isolator, which consists of a tripod mechanism. A vertically translating payload of mass m rests on a vertical spring of stiffness k_v; three oscillating rods of length L connect the payload to three pushrods through spherical joints. Each pushrod compresses a horizontal spring of stiffness k_h. The rods are angularly spaced at 120 degrees from each other, and the spring preload can be adjusted by varying displacements δ_v and δ_h for the vertical and horizontal springs, respectively.
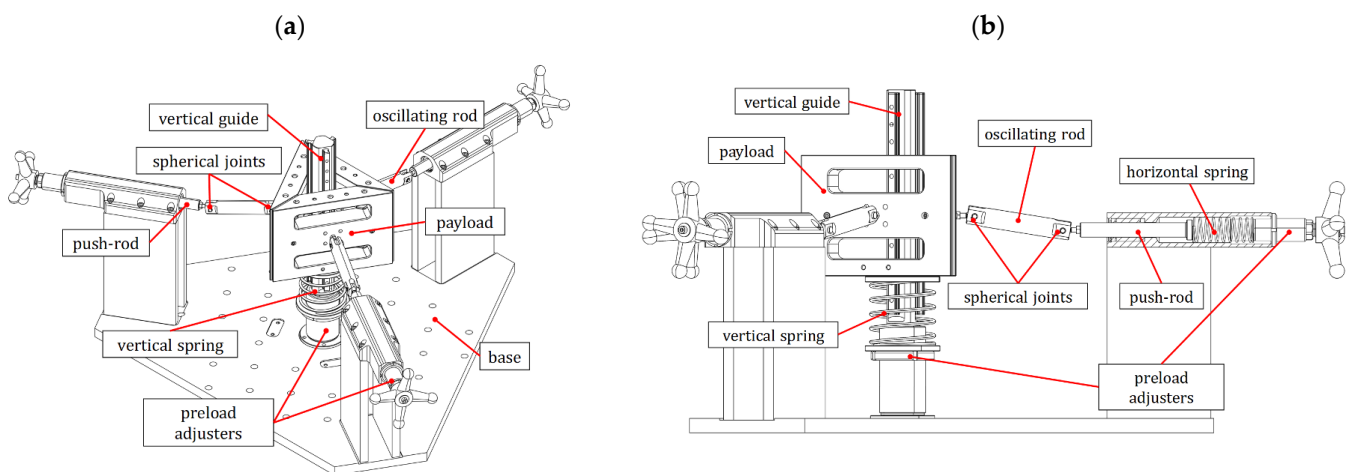
(a) **(b)**

Figure 1. Tripod isolator with HSLDS characteristics: (**a**) isometric and (**b**) lateral views.

Figure 2 shows the lumped parameter model employed to determine the static characteristics of the isolator, where the cumulative effect of the three horizontal springs functioning in parallel is modeled as a single horizontal spring with equivalent stiffness $3 \times k_h$, y denotes the payload displacement, θ is the actual angle between the rod and the horizontal line, and F is the generic external static force.
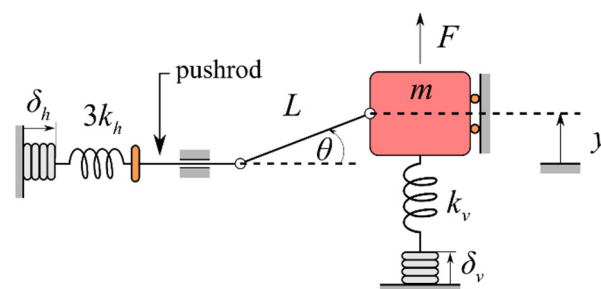

Figure 2. Lumped parameter model, static analysis.

The static behavior of the nonlinear isolator is governed by the equation,

$$F - F_s(y) = 0 \tag{1}$$

where $F_s(y)$ is the equivalent restoring force in the vertical direction. The horizontal springs are assumed to be purely compressive springs, i.e., they are unable to handle tractive forces. When the relative displacement y reaches a critical value y_{cr}, the pushrod detaches from the spring, directly influencing the restoring force, which can be expressed as a piecewise function. Thus, by introducing the following nondimensional parameters

$$\hat{y} = \frac{y}{L}, \qquad\qquad r = \frac{k_h}{k_v}, \\ \hat{\delta}_v = \frac{\delta_v}{L}, \qquad\qquad \hat{\delta}_h = \frac{\delta_h}{L}. \tag{2}$$

the nondimensional restoring force of the mechanism can be formulated as,

$$\frac{F_s(y)}{k_v\, L} = \hat{F}_s(\hat{y}) = \begin{cases} \hat{y} - \hat{y}_0 - \hat{\delta}_v - 3\,r\left[\hat{\delta}_h - \left(\sqrt{1-\hat{y}_0^2} - \sqrt{1-\hat{y}^2}\right)\right]\frac{\hat{y}}{\sqrt{1-\hat{y}^2}} & |\hat{y}| \le |\hat{y}_{cr}| \\ \hat{y} - \hat{y}_0 - \hat{\delta}_v & |\hat{y}| > |\hat{y}_{cr}| \end{cases} \tag{3}$$

where $\hat{y}(0) = \hat{y}_0$ is the initial position of the payload. The critical displacement $\hat{y}_{cr}$, which is dependent on $\hat{\delta}_h$, is found by considering the null deflection of the horizontal spring,

$$\hat{\delta}_h - \sqrt{1-\hat{y}_0^2} + \sqrt{1-\hat{y}^2} = 0 \rightarrow \hat{y}_{cr} = \sqrt{1 - \left(\sqrt{1-\hat{y}_0^2} - \hat{\delta}_h\right)^2} \tag{4}$$

It is important to note that $\hat{F}_s(\hat{y})$ is defined without considering the detachment of the payload from the vertical spring, as this condition is not relevant for describing the experimental observation shown in the results section.

Figure 3 shows how the preload of the horizontal springs affects the restoring force $\hat{F}_s(\hat{y})$: the system can be tuned to function as an HSLDS mechanism for small $\hat{\delta}_h$ values or a QZS system for large $\hat{\delta}_h$ values. Specifically, by differentiating Equation (3) with respect to the displacement $\hat{y}$, the equivalent vertical stiffness reads,

$$\hat{k}_s(\hat{y}) = \frac{d}{d\hat{y}}\hat{F}_s = \begin{cases} 1 - 3\,r\left[\dfrac{\hat{\delta}_h - \sqrt{1-\hat{y}_0^2} + \sqrt[3]{(1-\hat{y}^2)^2}}{\sqrt[3]{(1-\hat{y}^2)^2}}\right] & |\hat{y}| \le |\hat{y}_{cr}| \\ 1 & |\hat{y}| > |\hat{y}_{cr}| \end{cases} \tag{5}$$

Assuming $\hat{y}_0 = 0$, the minimum stiffness of the mechanism is obtained by evaluating $\hat{k}_s(\hat{y})$ for $\hat{y} = 0$, giving

$$\hat{k}_{s,min} = \hat{k}_s(0) = 1 - 3\,r\,\hat{\delta}_h \tag{6}$$

From Equation (6), depending on the value of $\hat{\delta}_h$, it is possible to observe that, in the neighborhood of the static equilibrium configuration, the system behaves in the following three ways:

- if $\hat{k}_{s,min} < 0$, the system presents a negative stiffness nonlinear spring;
- if $\hat{k}_{s,min} = 0$, the isolator works as a QZS mechanism;
- if $0 < \hat{k}_{s,min} < 1$, the isolator works as an HSLDS mechanism.

In order to study the dynamics of the isolator under base motion, the model depicted in Figure 4 is considered. The coordinate x represents the absolute displacement of the payload, x_b is the base displacement, and z denotes the relative displacement of the payload.
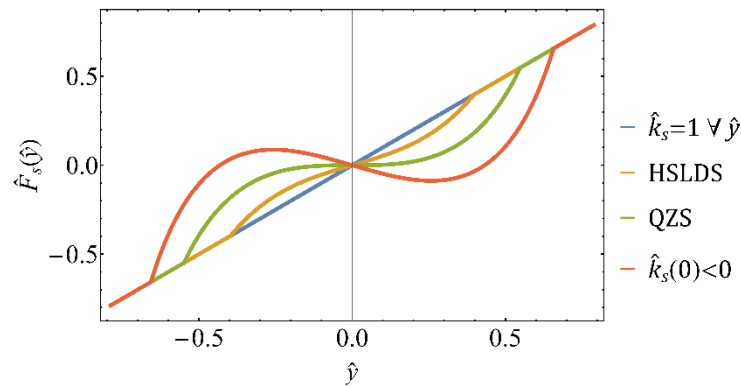
Figure 3. Non-smooth restoring force $\hat{F}_s(\hat{y})$ for different horizontal spring preloads (obtained assuming $\hat{y} = \hat{\delta}_v = 0$).
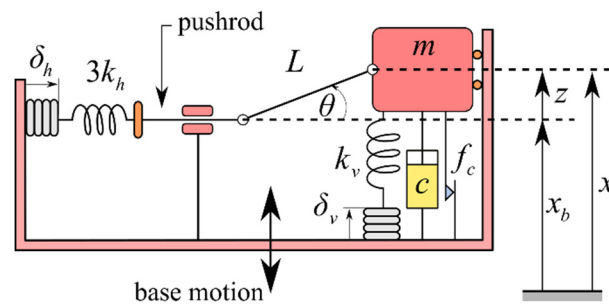

Figure 4. Lumped parameter model, dynamic analysis of the isolator under base motion.

Assuming that the system, under the action of the weight, is at rest in its static equilibrium position with the oscillating rods in a horizontal position, $z(0) = 0$, the restoring force $\hat{F}_s(\hat{z})$ is given by,

$$\hat{F}_s(\hat{z}) = \begin{cases} \hat{z} - \hat{\delta}_v - 3\,r\left(\hat{\delta}_h - 1 + \sqrt{1 - \hat{z}^2}\right)\dfrac{\hat{z}}{\sqrt{1 - \hat{z}^2}} & |\hat{z}| \leq |\hat{z}_{cr}| \\ \hat{z} - \hat{\delta}_v & |z| > |\hat{z}_{cr}| \end{cases} \tag{7}$$

where $\hat{z} = z/L$ is the nondimensional relative displacement of the payload. The critical value $\hat{z}_{cr}$ is determined as,

$$\hat{z}_{cr} = \sqrt{1 - \left(1 - \hat{\delta}_h\right)^2} \tag{8}$$

Following the approach adopted in Ref. [34] to account for different dissipation mechanisms, a dissipation function $\hat{F}_d(z, \hat{z}')$ is considered in the model and is assumed to be a combination of viscous and dry friction forces, i.e.,

$$\hat{F}_d(z, \hat{z}') = 2\,\zeta\hat{z}' + sign(\hat{z}')\,\hat{f}_c \tag{9}$$

where ζ and $\hat{f}_c = f_c(k_v\,L)^{-1}$ denote the viscous damping ratio and the normalized Coulomb friction force, respectively.

The governing equation of the 1-DoF lumped parameter system can now be written as,

$$\hat{z}'' + \hat{F}_d(z, \hat{z}') + \hat{F}_s(\hat{z}) + \hat{F}_g = -\hat{x}_b'' \tag{10}$$

where $(\cdot)'$ denotes derivatives with respect to the normalized time $\tau = \omega_n t$, $\omega_n = \sqrt{k_v/m}$ is the natural frequency of the linear oscillator, and $\hat{F}_g = mg(k_v\,L)^{-1}$ is the normalized weight.

In Equation (7), to satisfy the condition for static equilibrium, the vertical spring preload must be $\hat{\delta}_v = \hat{F}_g$, and by defining the auxiliary restoring force $\widetilde{F}_s(z) = \hat{F}_s(z) + \hat{F}_g$, the equation of motion for the tripod, Equation (10), can be rearranged to a simpler form,

$$\hat{z}'' + \hat{F}_d(z, \hat{z}') + \widetilde{F}_s(z) = -\hat{x}_b'' \tag{11}$$

Equation (11) is computationally stiff and potentially expensive to solve numerically due to the presence of discontinuous functions. Thus, a smoothing approach is used to simplify the analysis [35]: the piecewise restoring function $\hat{F}_s(z)$ is substituted by a continuous Sigmoid-like function $\gamma(\beta, \hat{z})$, while the dry friction term is approximated by the hyperbolic tangent $\sigma(\alpha, \hat{z}')$, where

$$\gamma(\beta, \hat{z}) = \frac{1}{1 + e^{-\beta(\hat{z} + \hat{z}_{cr})}} - \frac{1}{1 + e^{-\beta(\hat{z} - \hat{z}_{cr})}}$$
$$\sigma(\alpha, \hat{z}') = \frac{e^{\alpha \hat{z}'} - e^{-\alpha \hat{z}'}}{e^{\alpha \hat{z}'} + e^{-\alpha \hat{z}'}} \tag{12}$$

where α and β are parameters for controlling the smoothing functions.

Figure 5 shows the smoothing functions (12) for different values of α and β; see that for smoothing parameters of about 1000, both functions well approximate the step behavior while preserving the continuity conditions.
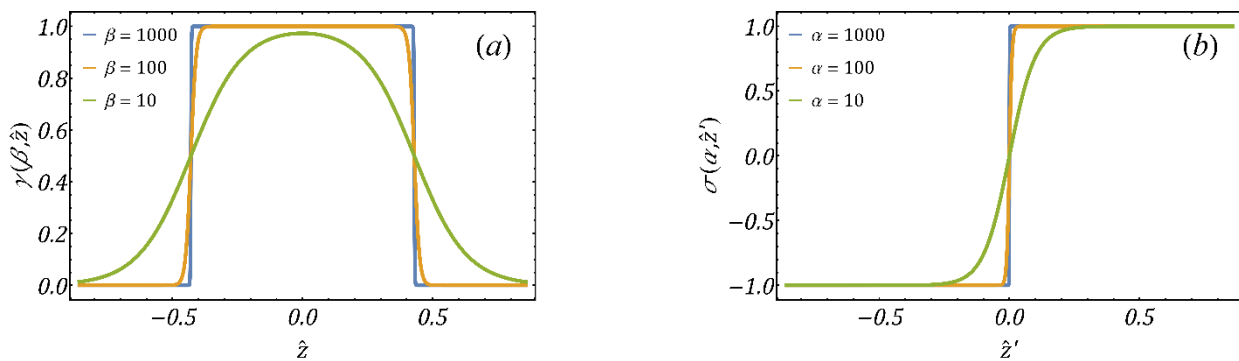

Figure 5. Smoothing functions: (**a**) sigmoid-based function and (**b**) hyperbolic tangent.

At this point, with the use of Equation (12), the equation of motion of the isolator can be rewritten in the state space as

$$\begin{cases} \hat{z}' = u \\ u' = -2\,\zeta u - \sigma(\alpha, u)\,\hat{f}_c - \hat{z} + 3\,r\left(\hat{\delta}_h - 1 + \sqrt{1 - \hat{z}^2}\right)\frac{\hat{z}}{\sqrt{1 - \hat{z}^2}}\gamma(\beta, \hat{z}) - \hat{x}_b'' \end{cases} \tag{13}$$

where $(\hat{z},\ u)$ are the state variables. Equation (13) is suitable for standard numerical integration. To this end, the Matlab solver ode23s for stiff ordinary differential equations [36] was used, assuming $\alpha = \beta = 1000$.

3. Experimental Setup and Shake Table Test

Experiments were conducted on a tripod isolator with payload mass $m = 20$ kg, oscillating rod length $L = 0.155$ m, vertical spring stiffness $k_v = 1848$ Nm^{-1}, and horizontal spring stiffness $k_h = 3747$ Nm^{-1}.

Figure 6a displays a schematic of the experimental setup: two piezoelectric accelerometers were used to measure the base and payload vibrations in the vertical direction; the seismic base motion was applied through a Dongling ET-40-370 shaker (40 kN peak force, 100 g maximum acceleration, 500 kg max static payload) controlled by a closed-loop algorithm, and signals were acquired using the LMS Scadas hardware with Testlab software.
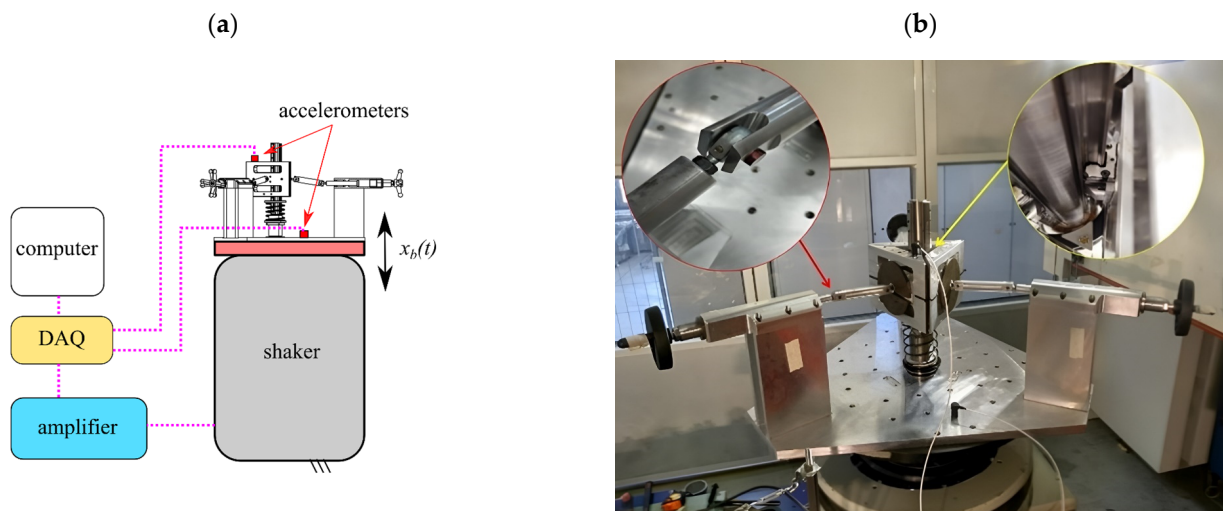
Figure 6. Shaking table tests: (**a**) schematic of the experimental setup, and (**b**) HSDLS mounted on the shaker.

Using the base and payload measurements, the absolute acceleration transmissibility was evaluated through the following expression,

$$T = \left| \frac{\text{RMS}(\ddot{x})}{\text{RMS}(\ddot{x}_b)} \right| \tag{14}$$

where RMS stands for root mean square.

3.1. Harmonic Excitation Tests

Stepped sine tests were carried out to evaluate the transmissibility *T* of the isolator. Using the Siemens SCADAS Mobile system and the Siemens Testlab control software (Sine Control module), the shaker base motion was controlled in terms of vertical acceleration amplitude $\left| \ddot{x}_b \right|$ and forcing frequency f_Ω, as shown in Figure 7. To assess the isolator's nonlinear characteristics, f_Ω was swept in the range of 0.5–10 Hz, both forward and backward. A variable frequency step Δf_Ω was chosen to span the resonance region with suitable frequency resolution, and for each frequency step, 120 periods of excitation were recorded with a sampling frequency of 400 Hz.
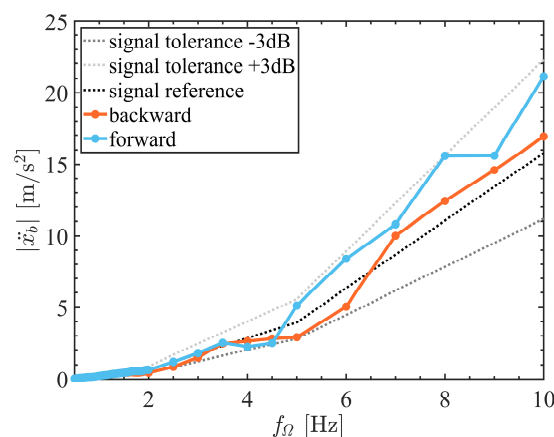

Figure 7. Harmonic excitation test. Shaker base acceleration amplitude $\left| \ddot{x}_b \right|$ at each frequency step for both backward and forward frequency sweep.

Controlling the shaking table at very low frequencies was demanding and critical due to the strict limitations on the maximum allowed displacement of the table (i.e., 51 mm, peak-to-peak). To address this limitation and ensure satisfactory control, the reference acceleration amplitude of the shaker base (black dotted line in Figure 7) was linearly varied at each step, with details about its slope provided in Table 1.

Table 1. Harmonic excitation test. Frequency step resolution and acceleration slope variations for each frequency range.

Frequency range f_Ω [Hz]	0.5–1.05	1.05–2	2–5	5–10
Frequency step Δf_Ω [Hz]	0.050	0.025	0.5	1
Slope of reference acceleration [m s^{-2} Hz^{-1}]	0.39	0.39	1.10	2.37

The investigated test cases are detailed in Table 2 and, more specifically, the following observations can be made:

- Each test is defined by a specific horizontal spring preload δ_h;
- Before each experimental test, the isolator's static equilibrium position, characterized by having horizontal rods, $z(0) = 0$, was imposed by adjusting the vertical spring preload δ_v. According to Equation (5), this angle was selected to provide the minimum stiffness around the static equilibrium position;
- To study the behavior of the isolator under HSLDS conditions for all the investigated cases, the displacement δ_h was kept below the QZS threshold given by Equation (6), $L(3\,r)^{-1}$ = 25 mm;
- Cases where $\delta_h > 12$ mm were excluded because payload oscillations with amplitudes exceeding the maximum allowed stroke were observed, causing the premature end of the test;
- The natural frequency of the system can be obtained by the linearization of the restoring force, Equation (7), using the Taylor series. Considering Case 1 as a reference, a reduction in natural frequency of 22% and 27% was achieved for Case 2 and Case 3, respectively.

Table 2. Parameters of the HSLDS isolator for the three investigated cases.

Parameter	Case 1	Case 2	Case 3
Horizontal spring preload δ_h [mm]	0	10	12
Total preload $3\,k_h\delta_h$ [N]	0	112.4	134.9
Natural frequency [Hz]	1.53	1.19	1.11

Figure 8a shows the transmissibility for a null preload. In this case, only the linear vertical spring contributes to the restoring force. In fact, the isolator behaves like a linear oscillator, except for the presence of dry friction, resulting in stiction at low frequencies when inertia is insufficient to overcome the friction force, as shown in the detailed view. By increasing the preload on the horizontal springs to 112.4 N, Figure 8b, a hardening nonlinearity is introduced. The tangent stiffness around the equilibrium position is reduced, leading to a lower natural frequency of the system. Additionally, the preload affects stick-slip thresholds: the greater the preload, the less relevant the role of dry friction becomes. Considering Figure 8c, where $3k_h\delta_h$ = 134.9 N, the stiction phenomenon disappears, and at low frequencies, the transmissibility curves obtained in the case of forward and backward sweeps are perfectly overlapped, except in the multiple-valued jump up/down region. In all the investigated cases, the transmissibility obtained using the lumped parameter model shows excellent agreement with the experimental measurements and is able to capture the stiffness variation due to the loss of contact between the pushrods and the horizontal springs. Regarding the hysteretic phenomenon at low frequencies, the dry friction model

considered in Equation (9) is not able to fit the experimental results for a narrow region in the case of null preload.
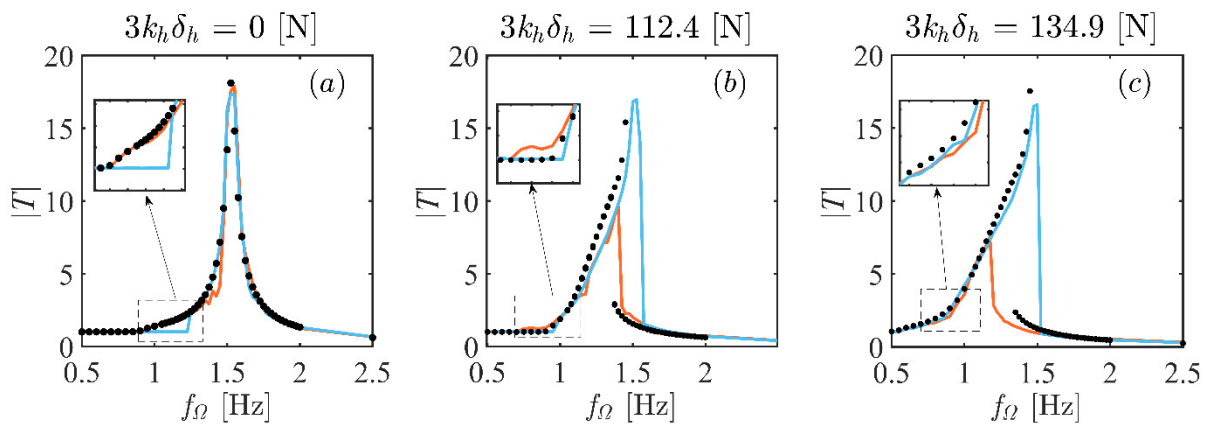

Figure 8. Magnitude of the transmissibility for different values of the horizontal springs preload: (**a**) 0 N, (**b**) 112.4 N, and (**c**) 134.9 N. Detailed views show the evolution of the stiction phenomena among the test cases. (— forward and — backward sweep, ••• numerical solution).

Values of the damping ratio and the dry friction force adopted in the numerical model to fit the experimental data are given in Table 3. Variations in the damping coefficient must be sought in the different lubrication conditions between different tests and in the limitations of the linear viscous model considered herein. In fact, the motion of the horizontal links can lead to nonlinear dissipation terms [18]. On the other hand, the decrease in dry friction force is attributed to the load acting perpendicular to the linear guides. These guides are preloaded; consequently, as the payload oscillates, the forces exerted by the horizontal springs have a direct impact on the overall load normal to the linear ball bearings.

Table 3. Viscous damping ratio and dry friction force values obtained from the fits of the experimental transmissibility curves.

Parameter	Case 1	Case 2	Case 3
Viscous damping ratio ζ	0.015	0.008	0.020
Dry friction force f_c [N]	3.44	3.44	0.86

3.2. Earthquake Experimental Results

The experimental response of the tripod isolator to simulated earthquakes is presented in this section. The near-fault earthquake signals were obtained from the PEER database [37], and the experiments were conducted by controlling the shaker base using the Siemens SCADAS Mobile system and the Siemens Testlab control software (Single Axis Waveform Replication module) with the built-in online adaptive closed-loop control strategy. Two different test sets were carried out:

(i) Amplitude-scaled tests: the acceleration amplitude of the input signals was reduced to cope with the shaker limits (i.e., shaker base overtravel);

(ii) Time-scaled tests: the input signals were compressed in time to shift the earthquake energy content to higher frequencies in order to account for the limited suspended mass.

Focusing on the amplitude scale tests, time histories and spectra of the test acceleration signals are given in Figure 9a–f. Earthquake vibrations carry energy content at low frequencies; therefore, to reduce the noise components and prevent signal phase shifting, the acquired data were filtered using a fifth-order Butterworth low-pass digital filter with a cut-off frequency of 30 Hz.
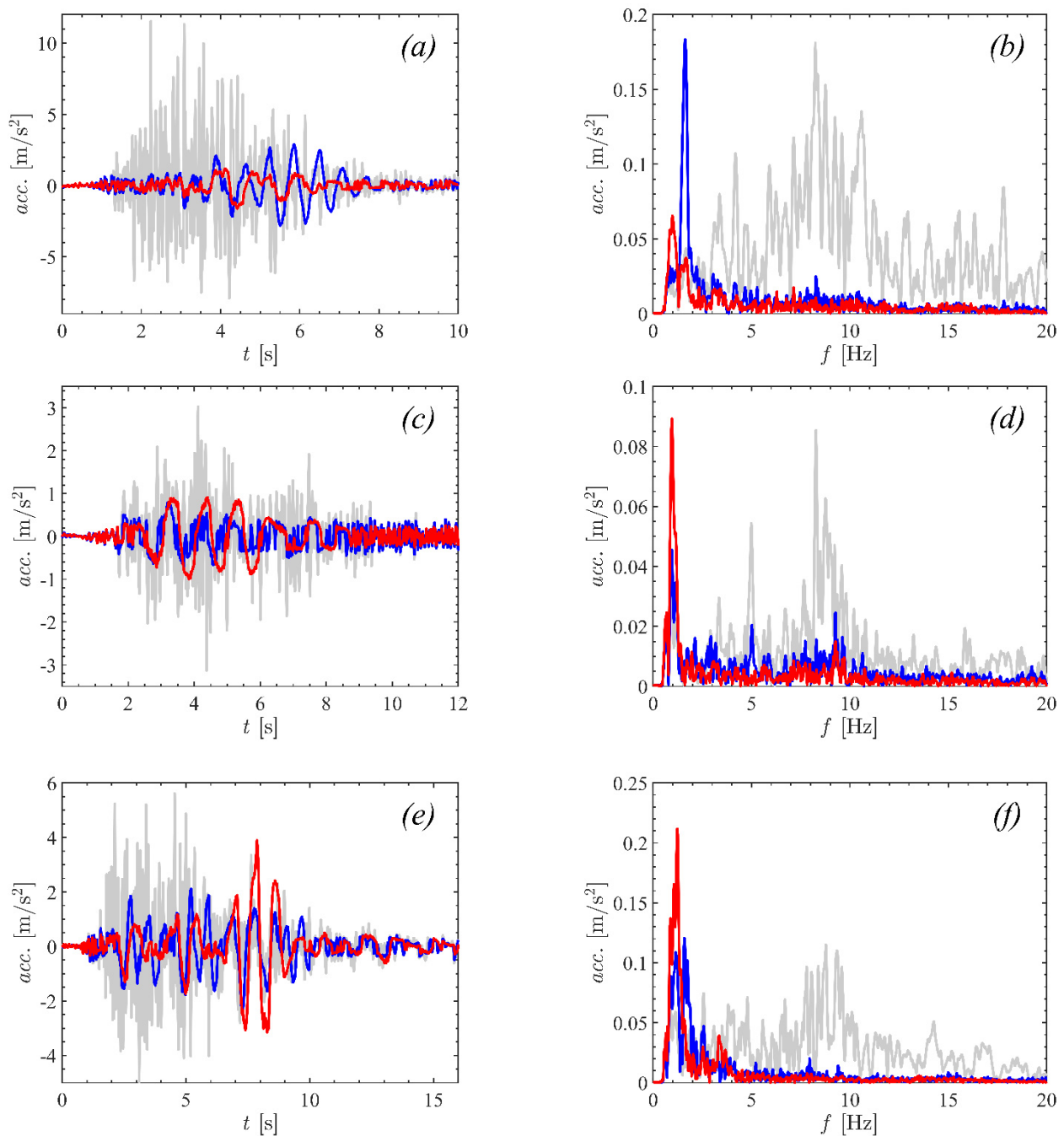
Figure 9. Amplitude-scaled tests. Acceleration time histories and spectra: (**a**,**b**) Christchurch, 70%; (**c**,**d**) Bam, 30%; and (**e**,**f**) Northridge, 90%. (— ground acceleration, — linear spring, and — HSLDS isolator).

Considering the Christchurch earthquake with an amplitude scaled by 70%, Figure 9a,b, the ground motion was particularly strong between [1–7 s], with a broadband spectrum governed by a peak at 8.24 Hz. Both the linear and the nonlinear (HSLDS Case 3, $3k_h\delta_h$ = 134.9 N) isolators were able to mitigate ground vibrations, Figure 9a, yet the HSLDS eliminated the resonance-like phenomenon exhibited by the linear system between [3.7–7.7 s], characterized by a harmonic component of the earthquake at 1.64 Hz, Figure 9b, hence close to the natural frequency of the system, which is 1.53 Hz according to Table 2. Conversely, for the Bam earthquake, with an amplitude scaling factor of 30%, the resonance of the HSLDS occurred in the range [2.5–6 s], Figure 9c. This behavior is attributed to the narrow frequency content of the ground motion, Figure 9d, localized at three frequencies:

0.95 Hz, 4.99 Hz, and 8.27 Hz. Despite the relatively small amplitude of the harmonic (0.036 m/s^2) at 0.95 Hz compared with the others, it was close enough to the HSDLS isolator resonance frequency (1.11 Hz) to induce strong payload oscillations. In Figure 9e, the linear and the HSLDS systems were compared under the Northridge earthquake, with an amplitude scaling factor of 90%. In this case, the HSLDS isolator reduction was higher than the linear system except between [6.5–9.3 s], where a sudden large amplitude oscillation of the HSDLS occurred. From the analysis of the frequency spectrum, Figure 9f, Northridge ground motion showed a double peak at 0.86 Hz and 1.15 Hz, causing the resonance of the HSDLS isolator. However, the frequency peaks were far enough from the resonance frequency of the linear system.

The results of the present section are summarized in the bar chart in Figure 10, where the peak acceleration and the RMS value provide a clear view of the performance of the linear and HSLDS isolators. Both systems were able to reduce ground vibrations in all the investigated cases, with the linear spring offering a higher reduction than the HSDLS isolator. However, for the Bam and Northridge cases, the HSDSL performance was conditioned by the activation of resonance-like phenomena.
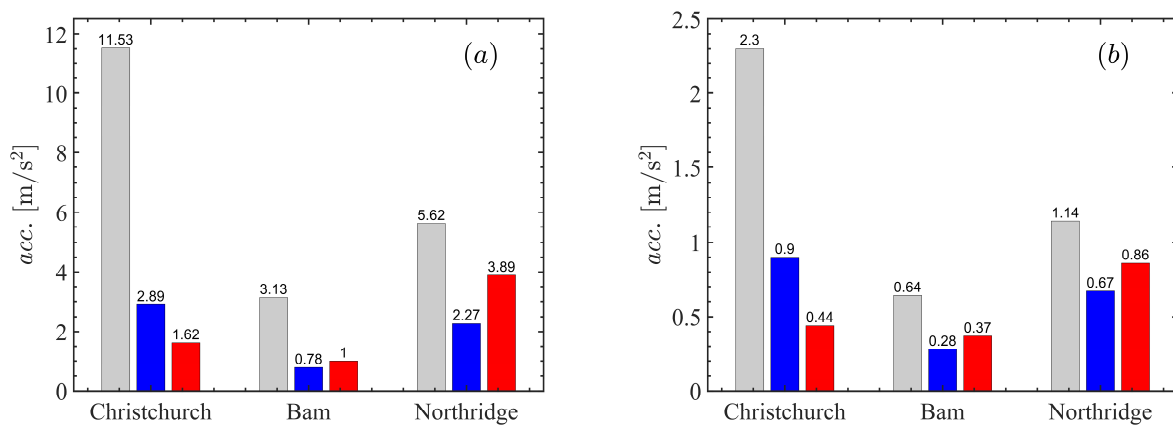

Figure 10. Amplitude-scaled test. Vertical acceleration: (**a**) maximum amplitude and (**b**) RMS. (— ground acceleration, — linear spring, and — HSLDS isolator).

Even though seismic isolators for actual buildings are designed to support large payloads and lead to very low resonance frequencies, the isolator under investigation was downsized for testing on a shake table having a limited payload of 300 kg. The limited value of the oscillating mass prevented the achievement of resonance frequencies below 1 Hz. Therefore, in order to perform realistic experiments on the downsized system, the original earthquake signals, having spectral energy at frequencies of about 1 Hz, were rescaled with respect to the time variable as $t_{scaled} = \xi t$, where $\xi > 1$ is the time-scaling factor. This scaling moves the signal spectral energy toward a higher frequency range that is more suitable for the downsized system. To determine a reasonable value for ξ, the following assumptions were considered: (i) small civil structures typically have resonance frequencies f_R of about 3–10 Hz [38–40], and (ii) the linear system in question had a resonance frequency near $f_S = 1.5$ Hz. Consequently, the time histories were scaled by a factor $\varepsilon = f_R f_S^{-1} = 2$.

Time histories and spectra of the time-scaled earthquake tests are presented in Figure 11a–f. It is important to note that, in these cases, the amplitude of the ground acceleration signals remained unaltered (i.e., 100%). Similar to the amplitude-scaled earthquake tests, a fifth-order Butterworth low-pass digital filter was used to reduce data noise. A larger cut-off frequency (100 Hz) was considered to account for the effect of time scaling, broadening the input signal energy content.
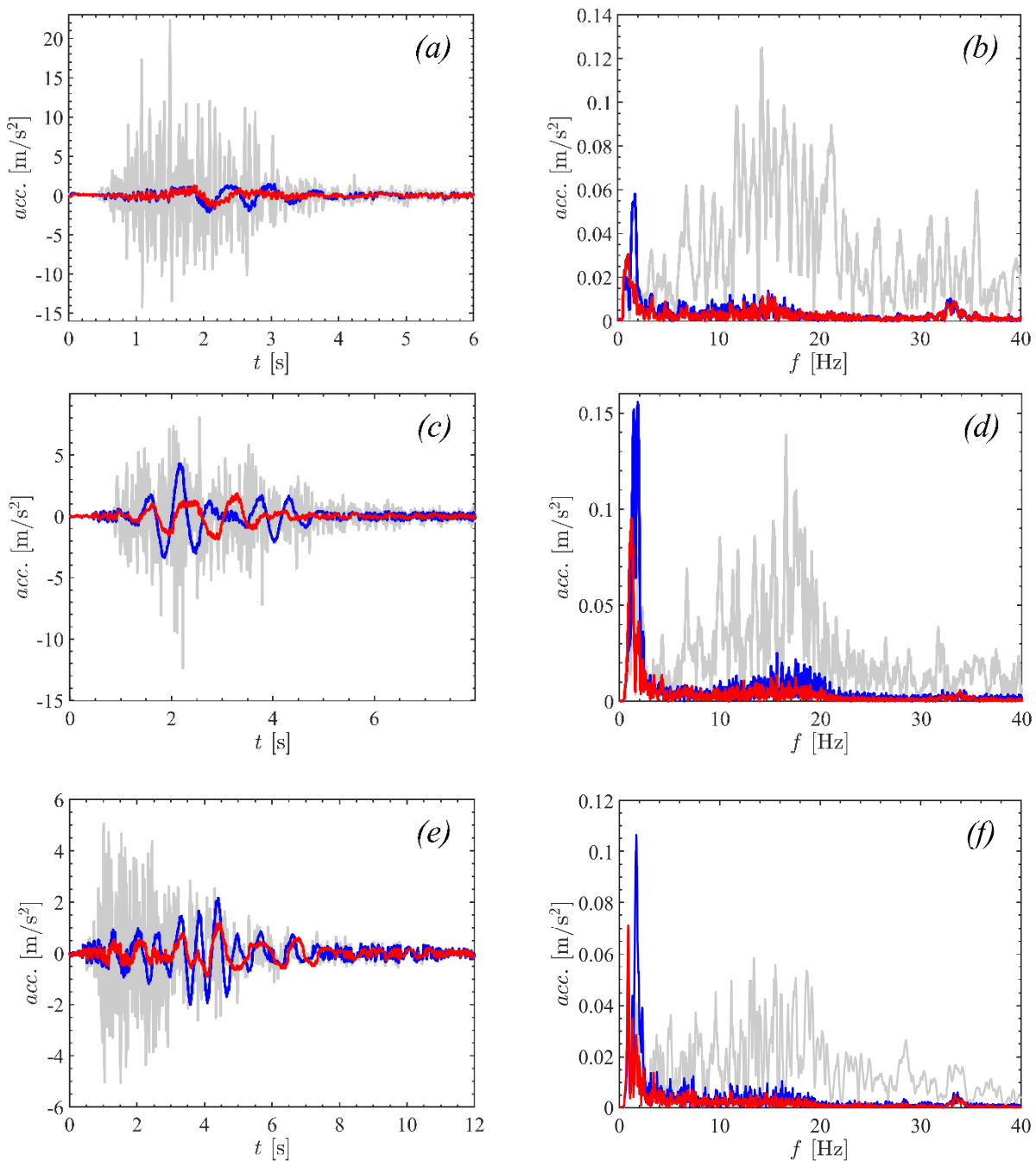
Figure 11. Time-scaled test. Acceleration time histories and spectra: (**a**,**b**) Christchurch, (**c**,**d**) Bam, and (**e**,**f**) Northridge. (— ground acceleration, — linear spring, and — HSLDS isolator).

In Figure 11a, both isolators behave similarly under the Christchurch earthquake, offering effective ground vibration reduction. Focusing on the acceleration RMS, an 81% reduction was achieved using the linear spring, while the HSDLS isolator demonstrated an 88% reduction. According to the spectrum, Figure 11b, the frequency content of the time-scaled Christchurch earthquake shifts to a higher frequency band, with a spectrum peak at 14.3 Hz, which is approximately one order of magnitude higher than the resonance frequencies of both the isolator configurations; thus, both the systems were working in the isolation regime.

Figure 11c shows the isolators' response to the Bam earthquake. The beneficial effects of the isolator are evident when the stiffness nonlinearity is retained. The payload's maximum acceleration amplitude measured with the HSLDS isolator (1.88 m/s^2) is lower

than the value observed for the payload carried by the linear spring (4.29 m/s^2). Moreover, in the latter case, periodic payload oscillations were activated from Bam low-frequency components at 1.43 Hz and 1.88 Hz, see Figure 11d.

The experimental response acceleration time histories and spectra considering the Northridge earthquake ground motion are shown in Figure 11e,f, respectively. Despite the time-scaling procedure, the input signal has a broad energy distribution up to 20 Hz, and the low-frequency components induced an increasing payload response between [0–4.4 s]. Yet, the HSLDS isolator showed a higher isolation degree than the simple linear spring, reducing the ground motion by 88% RMS, while an 81% RMS reduction was observed in the linear spring case.

By shifting the frequency content of the tested earthquakes to a higher frequency, the time-scaling procedure allowed both isolators to work under optimal conditions. From the comparison, it is evident that the HSLDS isolator consistently performed better than a linear system for all the tested signals, as shown in the bar charts given in Figure 12.
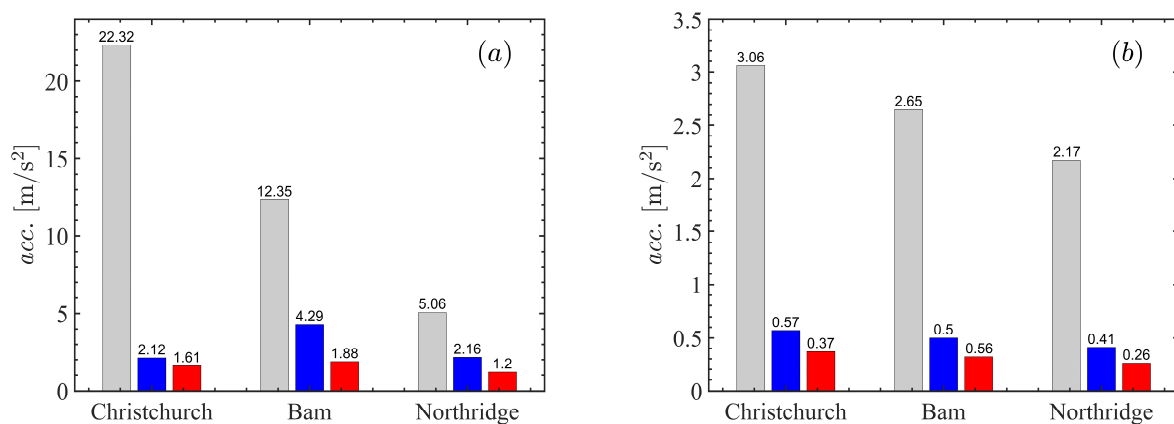

Figure 12. Time-scaled test. Vertical acceleration: (**a**) maximum amplitude and (**b**) RMS. (— ground acceleration, — linear spring, and — HSLDS isolator).

4. Concluding Remarks

In this study, the behavior of a nonlinear isolator under vertical base motion has been investigated. A three-dimensional tripod mechanism with tunable HSLDS characteristics was considered. A theoretical formulation incorporating a piecewise restoring force to approximate the behavior of compression springs was developed. Harmonic base motion experimental tests were conducted on a shaking table to assess the acceleration transmissibility, where different values of horizontal springs preload were used to tune the HSLDS characteristics. Additionally, ground vibration mitigation was evaluated under real-life seismic inputs. The concluding remarks of the work are summarized as follows:

The tunability of the proposed mechanism allows for adaptation to a wide range of loading conditions, making it a versatile solution for various applications.

(1) The numerically determined and experimental transmissibility exhibited noticeable agreement, underlining the importance of considering a piecewise nonlinear–linear restoring force to replicate the experimental observation;

(2) Harmonic excitation tests showed the limited capability of the Coulomb model to predict stiction phenomena, pointing out the need for refined friction and hysteresis models [41,42];

(3) Near-fault excitation tests revealed the beneficial effects of the HSLDS isolator in mitigating transmitted ground vibration to the payload. Results showed that a nonlinear isolator attained a higher vibration reduction than a linear spring isolator in four out of six investigated earthquakes;

(4) Experimental results align with existing literature [34], reinforcing the concept of the HSLDS mechanism as an effective means to prevent damage to sensitive objects;

(5) Insights into passive isolation systems are provided, revealing their susceptibility to resonance and emphasizing the importance of careful tuning to meet the safety requirements of suspended payloads.

Author Contributions: Conceptualization, S.I. and B.M.; methodology, all authors have contributed to the research methodology; software, G.I.; validation, G.I.; formal analysis, G.I., A.Z. and F.P.; investigation, G.I., A.Z. and F.P.; resources, F.P.; data curation, G.I. and F.P.; writing—original draft preparation, G.I., A.Z. and F.P.; writing—review and editing, F.E.-M., Y.M., S.I. and B.M.; visualization, G.I.; supervision, S.I. and F.P.; project administration, S.I.; funding acquisition, S.I. All authors have read and agreed to the published version of the manuscript.

Data Availability Statement: Data are available on request.

Conflicts of Interest: The authors declare no conflicts of interest.

References

1. Doocy, S.; Daniels, A.; Packer, C.; Dick, A.; Kirsch, T.D. The human impact of earthquakes: A historical review of events 1980-2009 and systematic literature review. *PLoS Curr.* **2013**, *5*, ecurrents.dis.67bd14fe457f1db0b5433a8ee20fb833. [CrossRef] [PubMed]
2. Parulekar, Y.M.; Reddy, G.R. Passive response control systems for seismic response reduction: A state-of-the-art review. *Int. J. Struct. Stab. Dyn.* **2009**, *9*, 151–177. [CrossRef]
3. Inman, D.J. *Engineering Vibration*, 4th ed.; Pearson International Education (Prentice Hall): Upper Saddle River, NJ, USA, 2013.
4. Abolfathi, A.; Brennan, M.J.; Waters, T.P.; Tang, B. On the effects of mistuning a force-excited system containing a quasi-zero-stiffness vibration isolator. *J. Vib. Acoust.* **2015**, *137*, 044502. [CrossRef]
5. Sarlis, A.A.; Pasala, D.T.R.; Constantinou, M.C.; Reinhorn, A.M.; Nagarajaiah, S.; Taylor, D.P. Negative Stiffness Device for Seismic Protection of Structures. *J. Struct. Eng.* **2013**, *139*, 1124–1133. [CrossRef]
6. Sarlis, A.A.; Pasala, D.T.R.; Constantinou, M.C.; Reinhorn, A.M.; Nagarajaiah, S.; Taylor, D.P. Negative Stiffness Device for Seismic Protection of Structures: Shake Table Testing of a Seismically Isolated Structure. *J. Struct. Eng.* **2016**, *142*, 04016005. [CrossRef]
7. David, L.P. Negative-stiffness-mechanism vibration isolation systems. In *Vibration Control in Microelectronics, Optics, and Metrology*; SPIE: Bellingham, WA, USA, 1992; Volume 1619. [CrossRef]
8. Gatti, G.; Brennan, M.J.; Tang, B. Some diverse examples of exploiting the beneficial effects of geometric stiffness nonlinearity. *Mech. Syst. Signal Process.* **2019**, *125*, 4–20. [CrossRef]
9. Molyneaux, W.G. Supports for vibration isolation. In *ARC/CP-322*; Aeronautical Research Council: London, UK, 1957.
10. Woodard, S.E.; Housner, J.M. Nonlinear behavior of a passive zero-spring-rate suspension system. *J. Guid. Control Dyn.* **1991**, *14*, 84–89. [CrossRef]
11. Carrella, A.; Brennan, M.J.; Waters, T.P. Static analysis of a passive vibration isolator with quasi-zero-stiffness characteristic. *J. Sound. Vib.* **2007**, *301*, 678–689. [CrossRef]
12. Carrella, A.; Brennan, M.J.; Waters, T.P. Optimization of a quasi-zero-stiffness isolator. *J. Mech. Sci. Technol.* **2007**, *21*, 946–949. [CrossRef]
13. Kovacic, I.; Brennan, M.J.; Waters, T.P. A study of a nonlinear vibration isolator with a quasi-zero stiffness characteristic. *J. Sound. Vib.* **2008**, *315*, 700–711. [CrossRef]
14. Brennan, M.J.; Kovacic, I.; Carrella, A.; Waters, T.P. On the jump-up and jump-down frequencies of the Duffing oscillator. *J. Sound. Vib.* **2008**, *318*, 1250–1261. [CrossRef]
15. Carrella, A.; Brennan, M.J.; Waters, T.P.; Lopes, V. Force and displacement transmissibility of a nonlinear isolator with high-static-low-dynamic-stiffness. *Int. J. Mech. Sci.* **2012**, *55*, 22–29. [CrossRef]
16. Cheng, C.; Li, S.; Wang, Y.; Jiang, X. Force and displacement transmissibility of a quasi-zero stiffness vibration isolator with geometric nonlinear damping. *Nonlinear Dyn.* **2017**, *87*, 2267–2279. [CrossRef]
17. Cheng, C.; Ma, R.; Hu, Y. Beneficial performance of a quasi-zero stiffness vibration isolator with generalized geometric nonlinear damping. *Noise Vib. Worldw.* **2021**, *52*, 59–71. [CrossRef]
18. Shahraeeni, M.; Sorokin, V.; Mace, B.; Ilanko, S. Effect of damping nonlinearity on the dynamics and performance of a quasi-zero-stiffness vibration isolator. *J. Sound. Vib.* **2022**, *526*, 116822. [CrossRef]
19. Jeong, B.; Cho, H.; Yu, M.F.; Vakakis, A.F.; McFarland, D.M.; Bergman, L.A. Modeling and measurement of geometrically nonlinear damping in a microcantilever-nanotube system. *ACS Nano* **2013**, *7*, 8547–8553. [CrossRef]

20. Den Hartog, J.P. Forced Vibration With Combined Viscous and Coulomb Damping. *Transcations Am. Soc. Mech. Eng.* **1930**, *9*, 801–817.
21. Ravindra, B.; Mallik, A.K. Hard duffing-type vibration isolator with combined Coulomb and viscous damping. *Int. J. Non Linear Mech.* **1993**, *28*, 427–440. [CrossRef]
22. Donmez, A.; Cigeroglu, E.; Ozgen, G.O. An improved quasi-zero stiffness vibration isolation system utilizing dry friction damping. *Nonlinear Dyn.* **2020**, *101*, 107–121. [CrossRef]
23. Liu, C.; Yu, K. Design and experimental study of a quasi-zero-stiffness vibration isolator incorporating transverse groove springs. *Arch. Civ. Mech. Eng.* **2020**, *20*, 67. [CrossRef]
24. Liu, C.; Zhang, W.; Yu, K.; Liu, T.; Zheng, Y. Quasi-zero-stiffness vibration isolation: Designs, improvements and applications. *Eng. Struct.* **2024**, *301*, 117282. [CrossRef]
25. Barbieri, M.; Ilanko, S.; Pellicano, F. Active vibration control of seismic excitation. *Nonlinear Dyn.* **2018**, *93*, 41–52. [CrossRef]
26. Samani, F.S.; Pellicano, F. Vibration reduction on beams subjected to moving loads using linear and nonlinear dynamic absorbers. *J. Sound. Vib.* **2009**, *325*, 742–754. [CrossRef]
27. Lan, C.C.; Yang, S.A.; Wu, Y.S. Design and experiment of a compact quasi-zero-stiffness isolator capable of a wide range of loads. *J. Sound. Vib.* **2014**, *333*, 4843–4858. [CrossRef]
28. Cheng, C.; Li, S.; Wang, Y.; Jiang, X. On the analysis of a piecewise nonlinear-linear vibration isolator with high-static-low-dynamic-stiffness under base excitation. *J. Vibroengineering* **2015**, *17*, 3453–3470.
29. Carrella, A.; Brennan, M.J.; Waters, T.P.; Shin, K. On the design of a high-static-low-dynamic stiffness isolator using linear mechanical springs and magnets. *J. Sound. Vib.* **2008**, *315*, 712–720. [CrossRef]
30. Dong, G.; Zhang, X.; Xie, S.; Yan, B.; Luo, Y. Simulated and experimental studies on a high-static-low-dynamic stiffness isolator using magnetic negative stiffness spring. *Mech. Syst. Signal Process.* **2017**, *86*, 188–203. [CrossRef]
31. Yan, G.; Zou, H.X.; Wang, S.; Zhao, L.C.; Wu, Z.Y.; Zhang, W.M. Bio-inspired vibration isolation: Methodology and design. *Appl. Mech. Rev.* **2021**, *73*, 1–21. [CrossRef]
32. Bian, J.; Jing, X. Analysis and design of a novel and compact X-structured vibration isolation mount (X-Mount) with wider quasi-zero-stiffness range. *Nonlinear Dyn.* **2020**, *101*, 2195–2222. [CrossRef]
33. Chong, X.; Wu, Z.; Li, F. Vibration isolation properties of the nonlinear X-combined structure with a high-static and low-dynamic stiffness: Theory and experiment. *Mech. Syst. Signal Process.* **2022**, *179*, 109352. [CrossRef]
34. Eskandary-Malayery, F.; Ilanko, S.; Mace, B.; Mochida, Y.; Pellicano, F. Experimental and numerical investigation of a vertical vibration isolator for seismic applications. *Nonlinear Dyn.* **2022**, *109*, 303–322. [CrossRef]
35. Kim, T.C.; Rook, T.E.; Singh, R. Effect of smoothening functions on the frequency response of an oscillator with clearance non-linearity. *J. Sound. Vib.* **2003**, *263*, 665–678. [CrossRef]
36. Shampine, L.F.; Reichelt, M.W. The MATLAB Ode Suite. *SIAM J. Sci. Comput.* **1997**, *18*, 1–22. [CrossRef]
37. *Peer Ground Motion Database*; Pacific Earthquake Engineering Research Center (PEER): Berkeley, CA, USA.
38. Eurocode 8. *Design of Structures for Earthquake Resistance—Part 3: Assessment and Retrofitting of Buildings*; Committee for Standardization: Brussels, Belgium, 2005; EN 1998-1.
39. Benedetti, D.; Carydis, P.; Pezzoli, P. Shaking table tests on 24 simple masonry buildings. *Earthq. Eng. Struct. Dyn.* **1998**, *27*, 67–90. [CrossRef]
40. Ceroni, F.; Sica, S.; Rosaria Pecce, M.; Garofano, A. Evaluation of the natural vibration frequencies of a historical masonry building accounting for SSI. *Soil. Dyn. Earthq. Eng.* **2014**, *64*, 95–101. [CrossRef]
41. Vaiana, N.; Rosati, L. Classification and unified phenomenological modeling of complex uniaxial rate-independent hysteretic responses. *Mech. Syst. Signal Process.* **2023**, *182*, 109539. [CrossRef]
42. Vaiana, N.; Rosati, L. Analytical and differential reformulations of the Vaiana–Rosati model for complex rate-independent mechanical hysteresis phenomena. *Mech. Syst. Signal Process.* **2023**, *199*, 110448. [CrossRef]